

Scanning Electrochemical Microscopy. 28. Ion-Selective Neutral Carrier-Based Microelectrode Potentiometry

Chang Wei and Allen J. Bard*

Department of Chemistry and Biochemistry, The University of Texas at Austin, Austin, Texas 78712

Geza Nagy and Klara Toth

Institute for General and Analytical Chemistry, Technical University of Budapest, Budapest, Hungary

Electrodes for scanning ion-selective potentiometric microscopy (or potentiometric SECM) were developed and used to image local concentration profiles of NH_4^+ , K^+ , and Zn^{2+} ions. Neutral carrier-based micropipet ion-selective electrodes with high spatial resolution ($\sim 2\text{--}3\ \mu\text{m}$) and fast response time ($\sim 300\ \text{ms}$) were fabricated and employed as potentiometric SECM tips, and high-resolution ion-selective images around micrometer-scale objects were obtained for selected model systems. This technique was also used to map enzyme activity and to measure concentrations within the diffusion layer of an ultramicroelectrode. Several methods are used to determine the absolute distance between tip and target on the basis of measurement of solution resistance using Ag/AgCl micropipet electrodes or potentiometric measurement of the steady-state concentration profile using ion-selective microelectrodes; the corresponding theories of both are presented. Dual-channel tips are also introduced for ion-selective potentiometric microscopy. In these, one channel operates as an ion-selective electrode and the other as a distance sensor. Quantitative concentration profiles can be obtained with knowledge of absolute tip position.

In recent years, scanning electrochemical microscopy (SECM) has been used for a wide range of applications in various electrochemical systems, especially in performing electrochemical measurements with high spatial resolution.¹⁻³ Compared to other types of scanning probe microscopy, one advantage of SECM is that it can provide information about the chemical nature and environment of the substrate of interest in addition to providing topographic images of the surface. In previous work from this laboratory and others, the SECM has been used in an amperometric mode to distinguish between insulating and conductive regions of substrates,⁴⁻⁷ to image the surface activity of a conductive substrate,⁸⁻¹⁰ to locate enzyme sites of surface-immobilized redox-active enzymes,^{11,12} and to map the local

concentration of an electroactive species.¹³ However, many interesting chemical systems are not accessible to amperometric techniques because the species of interest are not electroactive. For instance, alkali and alkaline earth metal ions important in biological systems cannot be quantified easily by voltammetry in aqueous media. Furthermore, amperometric detection of some electroactive species is limited by interference from background current. For example, direct amperometric determination of Zn^{2+} , a biologically and electrochemically important species, in aqueous media often suffers from interference by oxygen reduction and hydrogen evolution, and quantitative measurement of Zn^{2+} is possible only with an amalgam electrode as the detector. To broaden the scope of SECM, there is clearly a need to develop new types of sensors as scanning probes, e.g., potentiometric sensors, such as ion-selective microelectrodes (ISMEs). ISMEs have been developed for potentiometric determination of the local activity of different ions.¹⁴ Miniaturization of the electrode body has made possible the fabrication of ISMEs with tip diameters of micrometer and submicrometer dimensions. In the life sciences, ISMEs are routinely employed for the measurement of intracellular and extracellular ion activities in living cells, and many biologically important ions can be detected by potentiometric methods. Potentiometric SECM is better than amperometric detection for the quantitative measurement of the local concentration of a specific species, since a potentiometric tip electrode does not significantly change the concentration of the species to be detected. Moreover, potentiometric measurements allow direct calculation of the local ionic activity from a calibration curve, while in amperometric SECM, the tip signal is also affected by the surface topography of the substrate because the concentration is determined from the feedback current. Finally, potentiometric SECM generally provides better selectivity than its amperometric counterpart.

Several potentiometric SECM tips have been described.^{15,16} A Ag/AgCl microelectrode was used in potentiometric SECM experiments to probe ion fluxes of Ag^+ and Cl^- .¹⁵ Antimony-based pH microdisk electrodes were also fabricated and used to image

- (1) Bard, A. J.; Fan, F.-R. F.; Mirkin, M. V. In *Electroanalytical Chemistry*; Bard, A. J., Ed.; Marcel Dekker: New York, 1994; Vol. 18, p 243.
- (2) Bard, A. J.; Fan, F.-R. F.; Pierce, D. T.; Unwin, P. R.; Wipf, D. O.; Zhou, F. *Science* **1991**, *254*, 68.
- (3) Bard, A. J.; Denuault, G.; Lee, C.; Mandler, D.; Wipf, D. O. *Acc. Chem. Res.* **1990**, *23*, 357.
- (4) Wipf, D. O.; Bard, A. J.; Tallman, D. E. *Anal. Chem.* **1993**, *65*, 1373.
- (5) Wipf, D. O.; Bard, A. J. *Anal. Chem.* **1992**, *64*, 1362.
- (6) Kwak, J.; Bard, A. J. *Anal. Chem.* **1989**, *61*, 1794.
- (7) Kwak, J.; Bard, A. J. *Anal. Chem.* **1989**, *61*, 1221.

- (8) Engstrom, R. C.; Small, B.; Kattan, L. *Anal. Chem.* **1992**, *64*, 241.
- (9) Wipf, D. O.; Bard, A. J. *J. Electrochem. Soc.* **1991**, *138*, L4.
- (10) Wipf, D. O.; Bard, A. J. *J. Electrochem. Soc.* **1991**, *138*, 469.
- (11) Pierce, D. T.; Unwin, P. R.; Bard, A. J. *Anal. Chem.* **1992**, *64*, 1795.
- (12) Pierce, D. T.; Bard, A. J. *Anal. Chem.* **1993**, *65*, 3598.
- (13) Scott, E. R.; White, H. S.; Phipps, J. B. *Anal. Chem.* **1993**, *65*, 1537.
- (14) Ammann, D. *Ion Selective Microelectrodes: Principles, Design and Application*; Springer: New York, 1986.

local pH changes in several model chemical systems.^{16,17} However, potentiometric SECM thus far has been limited mainly to metal-based ISMEs (e.g., Ag or Sb) as tips. The advantages of these are fast response, easy fabrication (similar to that of conventional UMEs), and the possibility of passing current for the measurement of tip-to-target distance. However, these metal-based ISMEs can be used to detect only a few different types of ions (e.g., Ag⁺, Cl⁻, and H⁺), and the methods used to prepare these tips are not transferable to other ISMEs, since most ISMEs cannot be constructed in the same manner. The development of ISMEs clearly shows a trend toward liquid membrane microelectrodes based on the use of highly selective neutral carriers in a membrane.¹⁴ Indeed, liquid membrane, glass micropipet ISMEs have been used extensively in life sciences experiments. Such micropipet-based ISMEs would be particularly useful in SECM measurements and could broaden the applications of potentiometric SECM. A problem with such electrodes is the difficulty in determining the absolute position of the tip. Moreover, it is difficult to fabricate micropipet ISMEs that show high (μm) resolution and fast response. It is important both to determine the absolute distance between an ISME and the target under investigation to avoid damage to the tip and target if they touch and to extract quantitative information about concentration profiles near the surface. In some cases, optical microscopy can be used for this purpose, but this is usually not practical for tips of micrometer scale. Although double-barrel sensors with separate amperometric and potentiometric electrodes have been proposed for this purpose,¹⁸ no experimental results with these have been reported.

We describe here, for the first time, the use of micropipet ion-selective electrodes with neutral carriers in the potentiometric SECM mode. Several techniques are proposed for determination of the absolute tip-to-target distance based on dc measurement of solution resistance with Ag/AgCl micropipet electrodes or potentiometric measurement of steady-state concentration profiles using ISMEs. Potentiometric SECM tips with a dual-channel configuration are also introduced; in these, one channel works as an ion-selective electrode and the other as a distance sensor. The fabrication of micropipet-based K⁺, NH₄⁺, and Zn²⁺ electrodes is described, and their use to obtain high-resolution concentration profiles near micropipet or microdisk targets is presented.

THEORY

Distance Measurements with Micropipet Ag/AgCl Electrodes. In amperometric SECM with a conventional UME tip, the tip current can be recorded as a function of tip-to-substrate separation, d , as the tip approaches the substrate, and the normalized tip current can be employed to estimate absolute d .¹⁹ The absolute tip-to-substrate distance can also be found from ac impedance with a conventional UME in the absence of a mediator.²⁰ We show here that for a micropipet-based SECM tip, the

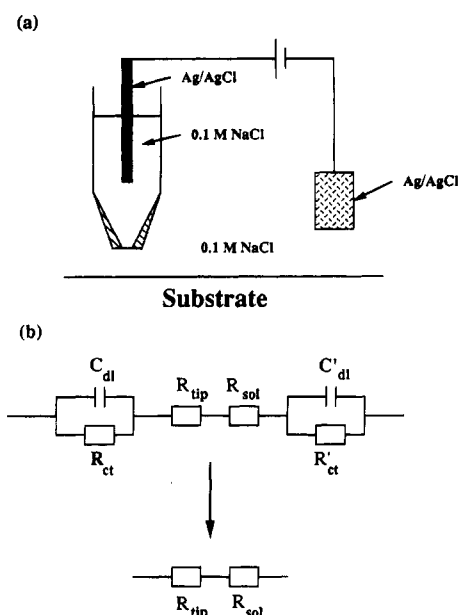
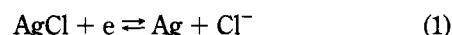


Figure 1. (a) Setup for distance measurements using a Ag/AgCl micropipet electrode. (b) Equivalent circuits representing the electrochemical processes described in eq 1.

tip-to-substrate distance in the absence of a mediator can be found from measurement of the dc solution resistance. This mediator-free technique is particularly useful for micropipet ion-selective electrodes with dual-channel tips. A similar effect has been applied in scanning ion conductance microscopy,^{21,22} although no quantitative treatment relating resistance and distance has previously been given.

A typical setup using a micropipet electrode for absolute tip-to-substrate distance measurement is shown in Figure 1a. A Ag/AgCl wire inserted into a micropipet serves as the SECM tip, and another Ag/AgCl electrode is placed in the bulk solution as the auxiliary/reference electrode. The micropipet is filled with the same electrolyte as in the bulk solution (e.g., 0.1 M NaCl) to avoid any liquid junction potential. While a constant dc voltage is applied between the two electrodes, the observed current is caused by the following reversible processes occurring at the electrode/electrolyte interfaces:



An equivalent circuit representing this electrochemical cell is depicted in Figure 1b. Because both electrodes have large surface areas relative to the aperture in the micropipet tip and the charge-transfer processes in eq 1 are rapid, one can neglect the contributions from the double-layer capacitance (C_{dl} , C'_{dl}) and charge-transfer resistance (R_{ct} , R'_{ct}) of the electrodes, and the equivalent circuit can be simplified to one in which the current is governed by the solution resistance:

$$R_t = R_{\text{tip}} + R_{\text{sol}} \quad (2)$$

where R_{tip} is the solution resistance inside the micropipet and R_{sol}

- (15) Denuault, G.; Troise Frank, M. H.; Peter, L. M. *Faraday Discuss.* **1992**, *94*, 23.
 (16) Horrocks, B. R.; Mirkin, M. V.; Pierce, D. T.; Bard, A. J.; Nagy, G.; Toth, K. *Anal. Chem.* **1993**, *65*, 1213.
 (17) Arca, M.; Horrocks, B. R.; Bard, A. J. *J. Phys. Chem.*, submitted.
 (18) Arca, M.; Bard, A. J.; Horrocks, B. R.; Richards, T. C.; Treichel, D. A. *Analyst* **1994**, *119*, 719.
 (19) Mirkin, M. V.; Fan, F.-R. F.; Bard, A. J. *J. Electroanal. Chem.* **1992**, *328*, 47.
 (20) Horrocks, B. R.; Schmidtke, D.; Heller, A.; Bard, A. J. *Anal. Chem.* **1993**, *65*, 3605.

- (21) Prater, C. B.; Hansma, P. K.; Tortonesi, M.; Quate, C. F. *Rev. Sci. Instrum.* **1991**, *62*, 2634.
 (22) Hansma, P. K.; Drake, B.; Marti, O.; Gould, S. A. C.; Prater, C. B. *Science* **1989**, *243*, 641.

is the external solution resistance between the tip and the reference electrode. R_t , the total solution resistance, can be calculated from the applied voltage and the measured current. As the micropipet tip approaches a substrate, R_{tip} remains unchanged, but R_{sol} increases because the substrate surface partially blocks the ionic pathway between tip and reference electrodes. The dependence of R_{sol} on d can be formulated on the basis of the analogy between the micropipet electrode and the microdisk electrode.²⁰ In amperometric SECM, Fick's equation for a microdisk electrode at steady state can be written as follows:

$$\nabla^2 c = 0 \quad (3)$$

with the steady-state tip current,

$$i_T = -nFD\nabla c \quad (4)$$

where c is concentration, n is the number of electrons transferred, D is the diffusion coefficient, and F is the Faraday constant. For the Ag/AgCl micropipet tip, in the absence of an ionic concentration gradient and a uniform value of the conductivity for the solution outside the tip, one can write

$$\nabla^2 \phi = 0 \quad (5)$$

with the current density,

$$j = -\kappa \nabla \phi \quad (6)$$

where ϕ is the potential and κ is the specific conductivity of the solution. Since the forms of eqs 3 and 4 for amperometric SECM are the same as those for the potential distribution, eqs 5 and 6, the following expression is readily obtained:²⁰

$$R_{sol,\infty}/R_{sol}(L) = i_T(L)/i_{T,\infty} \quad (7)$$

where $L = d/a$ is the normalized tip-to-substrate distance, a is the tip radius, $R_{sol}(L)$ is the external solution resistance of the micropipet, $i_T(L)$ is the feedback current of the microdisk at the normalized tip-to-substrate distance L , and $R_{sol,\infty}$ and $i_{T,\infty}$ represent these values with the tip far from the substrate. The distance dependence of the tip current due to the blocking effect by the substrate surface for a tip with $RG = 10$ has been given previously:

$$i_T(L)/i_{T,\infty} = 1/[0.292 + 1.5151/L + 0.6553 \exp(-2.4035/L)] \quad (8)$$

Thus, the solution resistance as a function of distance can also be formulated accordingly. The solution resistance between a disk electrode and an auxiliary electrode at infinity, equivalent to $R_{sol,\infty}$ here, is given by²³

$$R_{sol,\infty} = 1/4\kappa a \quad (9)$$

$R_{sol}(L)$ cannot be obtained directly, but it can be related to the experimentally determined total solution resistance R_t at L or far

(23) Newman, J. J. *Electrochem. Soc.* 1966, 113, 501.

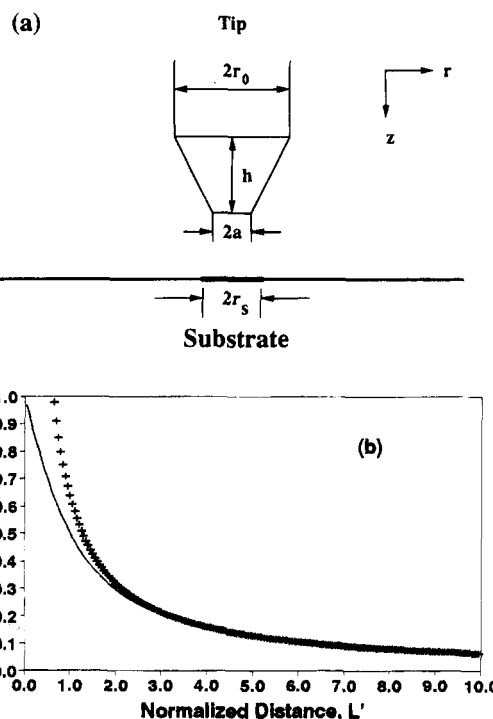


Figure 2. (a) Typical geometry of tip and target used in potentiometric SECM. The tip may be an ISME or a micropipet electrode. (B) Theoretical plots of a normalized concentration profile, $C(L')$, vs. normalized axial distance, $L' = d/r_s$, over the center of a target. The target was assumed to generate species at a steady state with a constant surface concentration. —, microdisk model, eq 16; + + +, approximate model, eq 17.

from the substrate:

$$\Delta R(L) = R_t(L) - R_{t,\infty} \quad (10)$$

Since R_{tip} is not a function of L ,

$$R_t(L) - R_{t,\infty} = R_{sol}(L) - R_{sol,\infty} = \Delta R(L) \quad (11)$$

By combining eqs 7, 8, 10, and 11, the distance dependence of solution resistance can be expressed as

$$\Delta R(L)/R_{sol,\infty} = -0.708 + 1.5151/L + 0.6553 \exp(-2.4035/L) \quad (12)$$

In eq 12, $\Delta R(L)$ is experimentally determined and $R_{sol,\infty}$ is obtained from eq 9. Thus, d can be determined from $\Delta R(L)$ from eq 12. Note that the distance dependence of the solution resistance is the same for both conductive and insulating substrates, since both show the same blocking effect, as long as the applied potential is sufficiently small that no faradaic reactions occur at the conductive substrate.

The sensitivity of this technique is limited by the relative values of R_{tip} and R_{sol} . If $R_{tip} \gg R_{sol}$, the change in $\Delta R(L)$ as a function of distance will not make a significant contribution to R_t , and $R_t \approx R_{tip}$. Clearly, $R_{tip}/R_{sol,\infty}$ should be kept as small as possible for good measurement sensitivity. For a tip with the geometry shown in Figure 2a,

$$R_{\text{tip}} = \rho/\pi \int_0^h \frac{dz}{\left[a + \frac{z}{h}(r_0 - a)\right]^2} \quad (13)$$

where z is the axial variable, r_0 is the radius of the tip capillary tube, h is the distance between the Ag/AgCl and the tip aperture, and ρ is the specific resistivity of the solution. Since $r_0 \gg a$, eq 13 becomes

$$R_{\text{tip}} = \rho h/\pi a r_0 \quad (14)$$

A comparison of the expressions for R_{tip} and $R_{\text{sol},\infty}$, eqs 9 and 14, shows that a decrease in $R_{\text{tip}}/R_{\text{sol},\infty}$ can be achieved by decreasing the ratio of h to r_0 . For the experiments in this study, h/r_0 was ≤ 5 , so $R_{\text{tip}}/R_{\text{sol},\infty} \leq 6$, which allowed for good sensitivity in the distance measurements.

Distance Measurements with Ion-Selective Microelectrodes. In potentiometric SECM with ion-selective microelectrodes, a neutral carrier-based ISME is used to measure the local concentration of the ion of interest around the target under investigation. The distance measurement using the technique described above cannot be used with such electrodes because the very high resistance of the ion-selective membrane causes R_{tip} to be large. In this case, dual-channel tips can be constructed with separate micropipet Ag/AgCl and ion-selective electrodes in which the Ag/AgCl electrode serves as the distance sensor. Since such electrodes are more difficult to construct, an alternative approach, in which a single ISME is used both for measurement of concentration and for distance determination, was used. If the system investigated by potentiometric SECM is at steady state, the measured concentration profile can be used to estimate the absolute tip-to-target distance. A small disk-shaped target with a constant surface concentration produces a steady-state concentration profile around the target that can be expressed as^{13,24}

$$c(r,z) = 2C_s/\pi \tan^{-1}(\sqrt{2}r_s/\{(r^2 + z^2 - r_s^2) + [(r^2 + z^2 - r_s^2)^2 + 4z^2r_s^2]^{0.5}\}^{0.5}) \quad (15)$$

where r and z are cylindrical coordinates (see Figure 2a), r_s is the target radius, and C_s is the surface concentration. At $r = 0$, and normalizing z and $c(r,z)$ with respect to r_s and C_s , one obtains the concentration profile in the axial (z) direction,

$$C(L) = 2 \tan^{-1}(1/L)/\pi \quad (16)$$

where $C(L) = c(0,d)/C_s$ and $L' = d/r_s$. When $L' \gg 1$ (i.e., $d \gg r_s$), $\tan^{-1}(1/L) \rightarrow 1/L$, so that eq 16 becomes

$$C(L) = 2/\pi L' \quad (17)$$

$$c(d) = 2r_s C_s/\pi d \quad (18)$$

A similar expression applies to a hemispherical target of radius r_s , except that the term $2r_s/\pi$ is replaced by r_s , as previously used for amperometric SECM.¹³ Figure 2b shows theoretical plots of $C(L)$ vs L' in which $C(L)$ has been calculated from eqs 16 and 17. The approximate model (eq 17) holds to $\leq 3\%$ when L' is

greater than 3.3. The absolute distance between tip and target, d , is generally unknown; however, in SECM measurements, d can be expressed as a function of the arbitrary displacement distance, d' , with a constant offset, A :

$$d = d' + A \quad (19)$$

Combining eqs 18 and 19 yields

$$d' = 2r_s C_s/\pi c(d) - A \quad (20)$$

Thus from a plot of d' vs $1/c(d)$, where a linear dependence is expected, the absolute distance offset A can be obtained from the intercept and the flux of the species from the slope. The surface concentration of the species can also be calculated from the slope, if the target radius is known. In principle, the absolute distance can also be determined by directly fitting the measured concentration profile into eq 16. Unfortunately, this method can only be used when the surface concentration is known. A similar method described in ref 13 can also be applied to determine the target size and the flux of the species if C_s or d is known. By combining the above method with the method in ref 13, both target size and surface concentration can be extracted from the concentration profile.

Similarly, for a disk-shaped target consuming a species at the diffusion-controlled rate (i.e., $C_s = 0$), the steady-state concentration profile established around the electrode can also be analytically described as follows:²⁵

$$c(r,z) = 2C_b/\pi \cos^{-1}(2r_s/\{[z^2 + (r_s + r)^2]^{0.5} + [z^2 + (r_s - r)^2]^{0.5}\}) \quad (21)$$

where C_b is the bulk concentration. Normalizing r , z , and $c(r,z)$ yields

$$C(R,L') = 2/\pi \cos^{-1}(2/\{[L'^2 + (1 + R)^2]^{0.5} + [L'^2 + (1 - R)^2]^{0.5}\}) \quad (22)$$

where $C(R,L') = c(r,z)/C_b$, $L' = d/r_s$, and $R = r/r_s$. At $R = 0$, the concentration profile in the axial direction is

$$C(L) = 2 \cos^{-1}[1/(L'^2 + 1)^{0.5}]/\pi \quad (23)$$

In this case, the absolute tip-to-target distance can be estimated by directly fitting the measured concentration profile to eq 23, because the bulk concentration C_b is usually known or easily measured; only one parameter, the normalized distance L' , is needed to fit eq 23.

EXPERIMENTAL SECTION

Chemicals and Materials. KCl, NaCl (Baker, Phillipsburg, NJ), Na₂HPO₄, FeCl₃ (Mallinkrodt, Paris, KY), KH₂PO₄, NH₄Cl (Fisher, Fair Lawn, NJ), LiCl (Aldrich, Milwaukee, WI), Ru(NH₃)₆Cl₃ (Strem, Newburyport, MA), and Zn(NO₃)₂ (Spectrum, Gardena, CA) were used as received and were reagent grade or better. Urease (EC 3.5.1.5; type IX from Jack Beans; 62 000 μM

(24) Saito, Y. *Rev. Polarogr.* **1968**, *15*, 177.

(25) Bond, A. M.; Oldham, K. B.; Zoski, C. G. *J. Electroanal. Chem.* **1988**, *245*, 71.

units/g), asparagine, and glutaraldehyde were obtained from Sigma (St. Louis, MO), and urea was received from Fisher. All chemicals used for the preparation of ion-selective membrane solutions and silanization of glass capillaries were obtained from Fluka, except *N*-phenyliminodiacetic acid *N,N'*-dicyclohexylbisamide, which was synthesized as previously reported.²⁶ Ag wire (0.25-mm diameter, 99.99%), Au wire (25- μ m diameter, 99.99%), and Ga metal (99.99%) were purchased from Aldrich, Goodfellow (Cambridge, England), and Johnson Matthey (Seabrook, NH), respectively. Borosilicate glass capillary tubes (single barrel, 1.50-mm o.d., 0.86-mm i.d.) were obtained from Sutter Instrument Co. (Novato, CA), and double-barrel (1.50-mm o.d., 0.84-mm i.d.) and thick septum θ (1.50-mm o.d., 1.02-mm i.d.) tubes were obtained from WPI (Sarasota, FL). Tris(hydroxymethyl)aminomethane (Tris, 99.0–99.5%, Sigma) was used for buffer solutions, and agar (MCB, Cincinnati, OH) was used in the preparation of the KCl salt bridges. Doubly distilled water (Milli-Q) was used for aqueous solutions in all cases.

Fabrication of Microelectrodes. *Ag/AgCl Micropipet Electrodes.* Ag/AgCl micropipet electrodes were constructed with either mechanically beveled glass tips or pulled glass capillaries. To produce a beveled glass tip, a clean, single-barrel, borosilicate glass tube was heat-sealed in a flame with a slow rotational motion to achieve a gradual tapering of the capillary bore toward the sealed end. The sealed end was polished back to expose a microscale circular opening in the middle of the glass surface and then beveled in a manner similar to that used for the fabrication of microdisk SECM tips.⁵ The resulting tip geometry was a micropipet with a glass diameter at the end about 10 times larger than that of the aperture, i.e., $RG = 10$. Pulled glass capillaries were pulled directly from clean borosilicate glass tubes using a CO₂ laser-based micropipet puller (Model P-2000, Sutter Instrument). The geometry of the tips (e.g., tip length or tip diameter) was controlled by selection of the puller parameters. To complete the electrode, a solution of 0.1 M NaCl or KCl was drawn into the micropipet through the tip, and a Ag/AgCl wire was inserted from the back. The Ag/AgCl wire was made either by passing anodic current through a Ag wire in KCl solution or by simply dipping the Ag wire into FeCl₃ solution.

Ion-Selective Microelectrodes. Two different types of micropipet ion-selective electrodes were fabricated for the potentiometric SECM measurements in this study; these are shown in Figure 3. Type A electrodes are conventional ISMEs which were pulled from single-barrel borosilicate glass tubes. Type B electrodes are dual-channel electrodes in which one channel is an ISME and the other, which serves as a distance sensor, is a Ag/AgCl electrode. These electrodes were fabricated using double-barrel or thick septum θ borosilicate glass tubes. Prior to use, the glass tubes were soaked in a 1:1 (v/v) mixture of concentrated sulfuric acid and 30% hydrogen peroxide for 24 h and then washed thoroughly with doubly distilled water and dried at 120 °C for 30 min. The laser-based puller was used to pull the single-barrel and thick septum θ glass tubes, and a heating coil-based puller (Stoetling) was used for double-barrel capillary pulling. The geometry of the micropipet was controlled as required. Typically the tip diameter was within the range of 1–20 μ m, and the ratio of the tip length to stem radius of the glass tube was made smaller than 5 (i.e., $h/r_0 \leq 5$). To silanize type A electrodes, the micropipets were first filled with

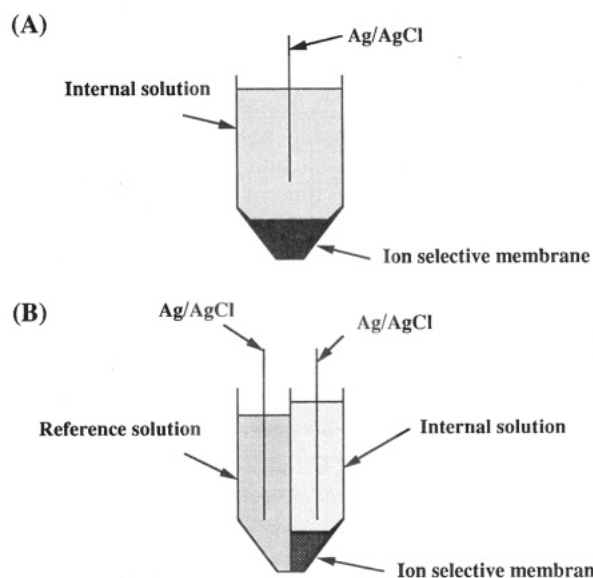


Figure 3. Schematic of the two types of ISMEs used. (A) Single-channel ISME. (B) Dual-channel Ag/AgCl micropipet electrode/ISME.

dimethyldichlorosilane vapor by syringe injection and then placed in a covered Petri dish which also contained a few drops of dimethyldichlorosilane. The silanization process was completed by allowing the glass surface of the micropipet to react with the vapor of the silanizing reagent for 2 h at 120 °C in an oven. The silanized micropipets were then connected to a water pump from the back to remove any remaining silanizing vapor inside the tip. By application of a slight overpressure with a syringe, the micropipets were back-filled with the proper internal filling solution (see below). The tips were then front-filled with the corresponding ion-selective membrane solution by capillary action and slight suction, and a Ag/AgCl wire was inserted to complete the ISME. For type B electrodes, only one of the two channels was silanized. This was done by introducing the silanizing vapor into one channel while continuously flushing nitrogen through the other channel. The channel not silanized was used for constructing the Ag/AgCl reference electrode as described above. The silanized channel was then back-filled with ion-selective membrane solution followed by the internal filling solution to form the ISME. The ionophores used in the ISMEs were BME 44 (K⁺ carrier, Fluka), nonactin (NH₄⁺ carrier, Fluka), and *N*-phenyliminodiacetic acid *N,N'*-dicyclohexylbisamide (Zn²⁺ carrier, ligand 4 in ref 26), and the corresponding internal filling solutions were 0.1 M KCl, 0.1 M NH₄Cl, and 0.001 M Zn(NO₃)₂, respectively. The ion-selective membrane solution was prepared using 5–7% (w/w) ionophore, 93–95% (w/w) *o*-nitrophenyl octyl ether, and 15–70 mol % potassium tetrakis(4-chlorophenyl)borate (relative to that of the ionophore).

Preparation of Targets. Micropipets and microdisks used as targets in this study were typically 1–25 μ m in diameter. In the experiment involving ion diffusion through a small opening, a U-shaped glass tube with a capillary at one end was used as the target. The capillary was pulled from a borosilicate glass tube with a tip diameter between 1 and 20 μ m. The U-tube was completely filled with the solution containing the ion of interest, and the capillary end was inserted into the cell through a hole drilled in the center of the cell base. The cell contained a blank solution with appropriate supporting electrolyte. Ag/AgCl wires were placed in the other end of the U-tube and in the bulk solution of the cell. By applying a dc potential between these two Ag/

(26) Lindner, E.; Horvath, M.; Toth, K.; Pungor, E.; Bitter, I.; Agai, B.; Toke, L. *Anal. Lett.* 1992, 25, 453.

AgCl electrodes, ions inside the U-tube were driven into the cell solution by migration.

For local measurement of enzyme activity, urease immobilized in capillaries served as targets, as described previously.¹⁶ Briefly, the pulled capillaries with a tip radius of 5–10 μm were dipped into a 25% glutaraldehyde solution so that a small amount of solution was drawn into the tip by capillary action. After about 10 min, the excess glutaraldehyde solution inside the tip was sucked out, and a urease solution of 25 mg/mL in phosphate buffer (pH 7) was introduced into the tip for 20 min to allow the formation of a solid gel containing enzyme at the tip. Further removal of excess glutaraldehyde was accomplished by soaking the capillary in 10 mM asparagine solution. The prepared urease target was then inserted into the base of the cell for experiments. Measurements were made at open circuit in 0.1 M Tris buffer solution (pH 7) containing 0.1 M urea.

For Zn^{2+} studies, a microdisk amalgam electrode was used as the target. To prepare such a target, a 25- μm -diameter gold wire was heat-sealed in a glass tube under vacuum by conventional techniques.²⁷ After polishing, the gold microdisk electrode was dipped into a mercury pool for a few seconds to allow the formation of amalgam at the Au surface. The resulting electrode was wiped on a piece of tissue paper to remove the excess mercury and then inserted into the cell as a working electrode for the electrodeposition of zinc (Ag/AgCl reference electrode and platinum foil counter electrode) from 50 mM Tris buffer solution (pH 7) containing 0.84 mM $\text{Zn}(\text{NO}_3)_2$ and 0.1 M NH_4Cl at -1.15 V. In all experiments, the SECM cell was made of Teflon and had a volume of about 4 mL.

Instrumentation. A slight modification was made to the basic instrumentation and electrochemical cell used for potentiometric SECM measurements, details of which have been given previously,¹⁶ to permit the use of a bipotentiostat. Briefly, a CE-1000 micropositioning device (Burleigh Instruments, Fishers, NY) connected to a PC via a DAC was used to control the movement of the tip via three piezoelectric inchworm motors. An electrochemical cell with the target of interest placed in the middle of the base was mounted on a horizontal stage. An EI-400 bipotentiostat (Ensmann Instruments, Bloomington, IN) and a high-impedance voltmeter (home-built)¹⁶ in conjunction with the PC were used for potential control and measurement. To avoid problems arising from the interactions between the bipotentiostat and the high-impedance voltmeter, the working electrode A lead in the bipotentiostat was left at open circuit and the potential of channel A was set at 0 V so that the reference electrode was forced to virtual ground. A common reference electrode could then be used for both amperometric and potentiometric measurements. The potential control of the targets (if necessary) was obtained through channel B. For potentiometric experiments, a salt bridge (with 3–5% agar gel containing 0.01 M KCl) was also employed between the reference electrode chamber and the test solution to reduce the possible interference from foreign ions. The electrodeposition and stripping of zinc employed a BAS 100B electrochemical analyzer with a BAS preamplifier (BAS, West Lafayette, IN).

RESULTS AND DISCUSSION

Distance Measurements. Experimental approach curves (change in solution resistance vs distance) for a Ag/AgCl

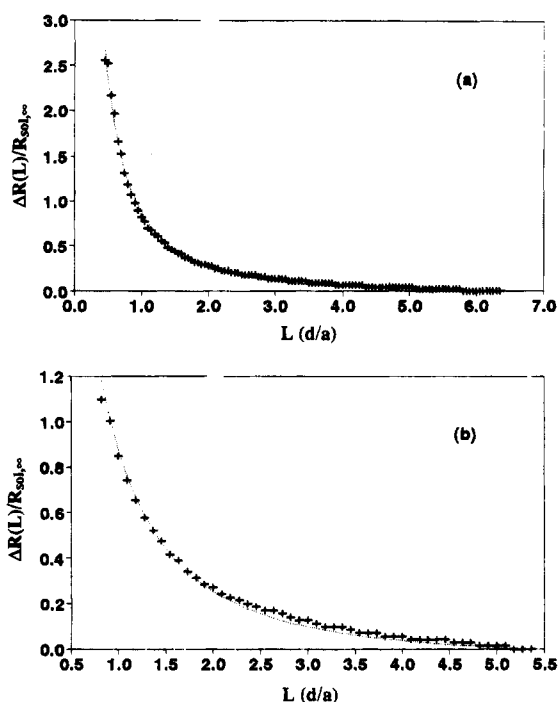


Figure 4. Solution resistance vs distance curves for a Ag/AgCl micropipet electrode over (a) Pt and (b) Teflon targets (setup shown in Figure 1a). Solution, 0.1 M KCl; applied voltage, 50 mV between the two Ag/AgCl electrodes; micropipet diameter, 20 μm ($RG = 10$). + + +, Experimental data; ···, theoretical curves.

micropipet electrode over Pt and Teflon surfaces are shown in Figure 4. These fit well the theoretical model, eq 12 (dotted line in Figure 4). The same dependence of solution resistance on distance is found for both the Pt and the Teflon substrates as expected. The micropipet electrodes have the advantage over microdisk electrodes for absolute distance calibration that no additional redox mediator is needed, and they are easier to fabricate,²⁸ especially for electrodes with submicrometer dimensions. For example, micropipets with nanometer-dimensioned apertures can be easily pulled from quartz tubes. The disadvantage for these electrodes is that the internal solution resistance of the micropipet may limit the sensitivity of the measurement.

The above method cannot be applied directly to the micropipet-based ISEs for distance measurement because of the high resistance of the ion-selective membrane at the tip. However, dual-channel tips with a separate ISME and distance sensor can be used. The approach curves, ΔR vs d , for a type B electrode over a target are essentially the same as those in Figure 4. Although the geometry of the dual-channel tip is somewhat different than that assumed in the model (e.g., $RG \neq 10$), the agreement with eq 12 was still sufficiently good to allow determination of d . Note that the Ag/AgCl electrode can also serve as a reference electrode for the ISME. In fact, double-barrel tips with separate Ag/AgCl reference microelectrode and ISME have been fabricated and used previously for the measurement of intracellular ion activity in order to avoid the membrane potential of a cell. Moreover, this type of dual-channel electrode minimizes problems with iR drop between sensor and reference electrode in systems with current flowing at the targets,¹⁵ since the reference electrode is only a few micrometers from the potentiometric sensor. How-

(27) Wightman, R. M.; Wipf, D. O. In *Electroanalytical Chemistry*; Bard, A. J., Ed.; Marcel Dekker: New York, 1988; Vol. 15, p 267.

(28) Lee, C.; Miller, C. J.; Bard, A. J. *Anal. Chem.* **1991**, *63*, 78.

(29) Nagy, G.; Toth, K.; Wei, C.; Bard, A. J., to be submitted.

ever, in the work described here, the current flow at the targets used was small (10^{-7} A or less), and the iR interference was negligible.

The steady-state concentration profile can also be used to estimate the absolute tip-to-target separation. A single-barrel ISME was used in this case to obtain both concentration and distance information. However, distance determined by the concentration profile requires the establishment of steady state at the target, while with the dual-channel electrodes, d is measured by an independent distance sensor. In the work presented here, either single-barrel (type A) or dual-channel (type B) ISMEs have been employed for the measurement of the concentration profile around the different targets of interest.

Characterization of Ion-Selective Microelectrodes. K^+ , NH_4^+ , and Zn^{2+} -selective electrodes with type A or B configuration were characterized. Potential vs concentration calibrations for all ISMEs used in this study were obtained. Typically, a linear dependence of the electrode potential on the concentration of the corresponding ionic species (10^{-5} to 0.1 M) was observed, with slopes of ~ 55 mV for K^+ and NH_4^+ and ~ 27 mV for Zn^{2+} , in good agreement with the theoretical values for monovalent and divalent ions. The stability of the ISMEs was also tested. Although the concentration response varied slightly among different electrodes, reproducible behavior was observed for any individual electrode, and the calibration plots were very similar on different days. In all SECM experiments, the ISMEs were calibrated both before and after the measurement in order to ensure the good performance of the electrodes. The selectivity of ISEs with the membrane materials used here has been documented.^{26,30}

A fast response time of the ISME is necessary in potentiometric SECM to obtain undistorted images. Different techniques have been described for the determination of the response time of ISEs.³¹ A simple method for the measurement of the electrode response time using the SECM setup with a type B electrode is illustrated in Figure 5a for a K^+ ISME. Briefly, the dual-channel tip was mounted on a tip holder in the SECM system to allow the scanning of the tip in the vertical (z) direction. The tip was first immersed in 0.1 M KCl solution and then withdrawn to form a thin film of KCl solution between tip and reference. In air, the tip potential slowly drifted in a positive direction due to the evaporation of water from the KCl solution at the tip, resulting in a tip potential different from that of the bulk solution. The response time of the ISME was then determined by rapidly plunging the tip into the 0.1 M KCl and recording the tip response as a function of time. In a typical response curve of a K^+ -selective electrode (Figure 5b), a steady potential was obtained within 300 ms after the electrode was brought into contact with the bulk solution (response time of ~ 10 ms/mV). This response time is fast enough to give undistorted information in potentiometric SECM at scan rates of up to $10 \mu\text{m/s}$. The other ion-selective electrodes employed in this study had response times of the same order of magnitude.

Ion-Selective Imaging with High Resolution. Potentiometric SECM with micropipet-based ISMEs is capable of monitoring and mapping local concentrations with high resolution. To illustrate this application, the flux of an ion through a $<20\text{-}\mu\text{m}$ opening was imaged, as described in detail in the Experimental

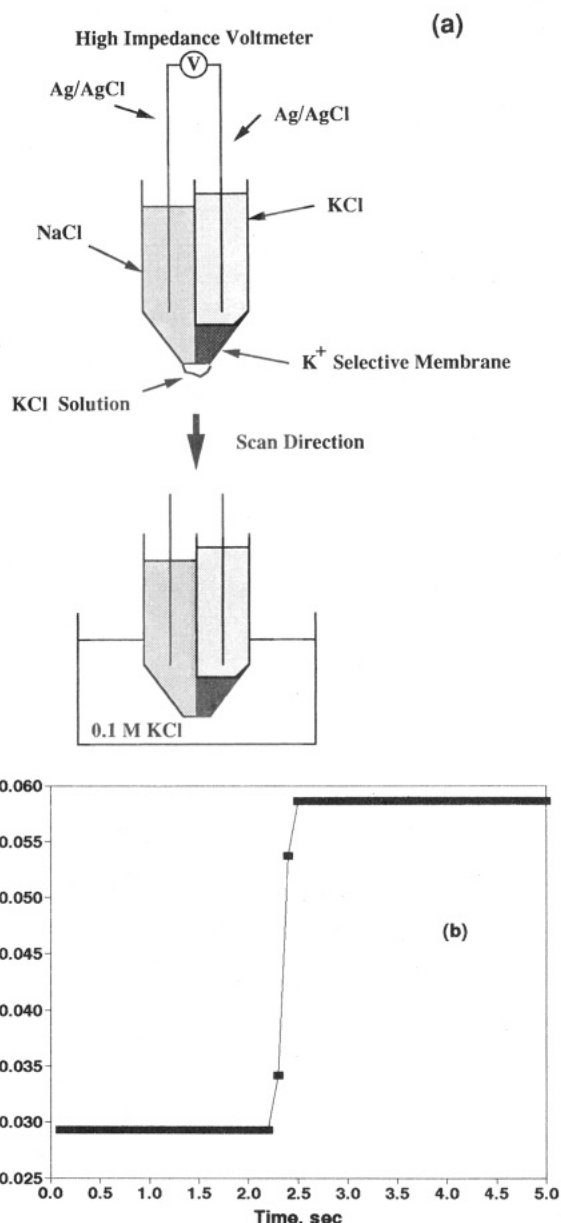


Figure 5. (a) Setup used for the measurement of ISME response time; scanning of the ISME was controlled via the SECM apparatus. (b) Plot of typical time response for a type B K^+ ISME.

Section. The U-tube was filled with the solution containing the ion to be imaged at a known concentration, while the cell contained only supporting electrolyte. By applying a dc voltage between the two Ag/AgCl electrodes, ion transport across the opening of the micropipet was driven by the electric field gradient. When a positive voltage was applied to Ag/AgCl in the U-tube, cations were driven toward the opening of the micropipet by migration and then diffused away from the opening into the bulk solution. The ion flux here was dominated by radial diffusion from the opening since an excess of supporting electrolyte was present. Thus a steady-state concentration profile of ions was established around the opening, and the local concentration could be obtained by scanning the corresponding ISME tip over the capillary aperture. Ion-selective imaging for NH_4^+ , K^+ , or Zn^{2+} around the target was studied with an inert supporting electrolyte. Based on selectivity considerations, LiCl, NaCl, and NH_4Cl were utilized as supporting electrolytes for the determination of NH_4^+ , K^+ , and Zn^{2+} , respectively. A typical experiment was conducted by first

(30) *Selectophore: Ionophores for Ion-Selective Electrodes and Optodes*; Fluka Chemika: Switzerland, 1991.

(31) Linder, E.; Toth, K.; Pungor, E. *Dynamics of Ion Selective Electrodes*; CRC Press: Boca Raton, FL, 1988.

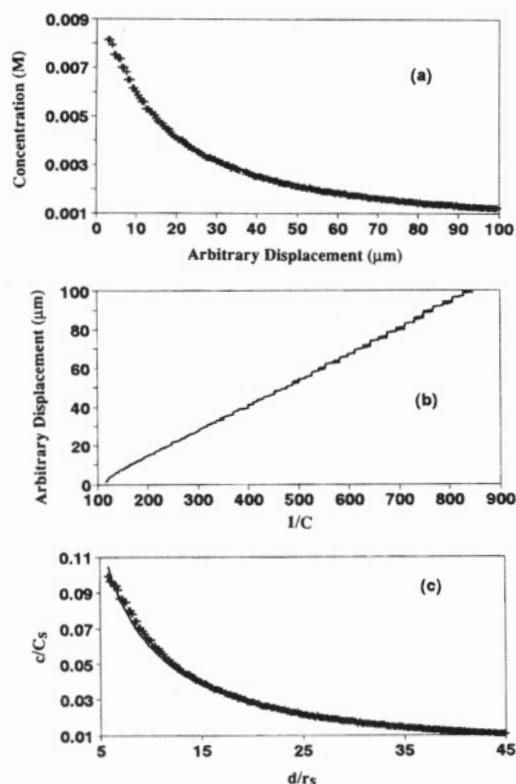


Figure 6. (a) NH_4^+ concentration profile above a 5- μm -diameter micropipet (in the z -direction) over the center of the source. Bulk concentration inside the micropipet, 0.1 M NH_4Cl ; outside, 0.1 M LiCl ; applied potential, 0.9 V; tip diameter of the NH_4^+ ISME, $\sim 1 \mu\text{m}$. (b) Corresponding plot of arbitrary displacement vs the reciprocal of NH_4^+ concentration. (c) Plot of normalized concentration vs normalized distance based on the parameters obtained from Figure 6b. ++, Experimental data; —, theoretical curve.

filling a capillary (the target) with the solution containing the ion to be determined and placing it in the base of the cell. The ISME tip was positioned roughly over the target aperture using the piezos with observation with a telescopic lens. The supporting electrolyte was then introduced, and a dc voltage was applied to establish a steady-state concentration profile of the test ion. The tip was positioned in the x - y plane by locating the position of maximum concentration, right above the target. The tip was then scanned in the vertical (z) direction. The z -direction concentration profile of the NH_4^+ (z -displacement vs d) at this position is shown in Figure 6a. Since a steady-state concentration is established around the small aperture, eq 15 can be applied to the system. If the distance between the tip and target is much larger than the radius of the target (e.g., $d > 3r_s$), eq 20 can be used to construct a plot of displacement vs $1/c$ from the data presented in Figure 6a. The resulting linear plot, shown in Figure 6b, allows one to establish the offset, 13 μm , and confirms the assumption of $d > 3r_s$, where $r_s = 2.5 \mu\text{m}$. The surface concentration of NH_4^+ at the target was calculated to be 0.083 M from the slope in Figure 6b and eq 20. While the surface concentration should be affected by the applied voltage between the two Ag/AgCl electrodes, the quantitative dependence was not established in this study. Plots of the normalized concentration (c/C_s) as a function of the normalized distance (d/r_s) for the experimental data are shown in Figure 6c; these show a good fit to the theoretical curve.

Images of the concentrations of NH_4^+ around a 5- μm -diameter aperture in 0.1 M LiCl at two different tip-to-target separations are shown in Figure 7. These images were obtained by rastering

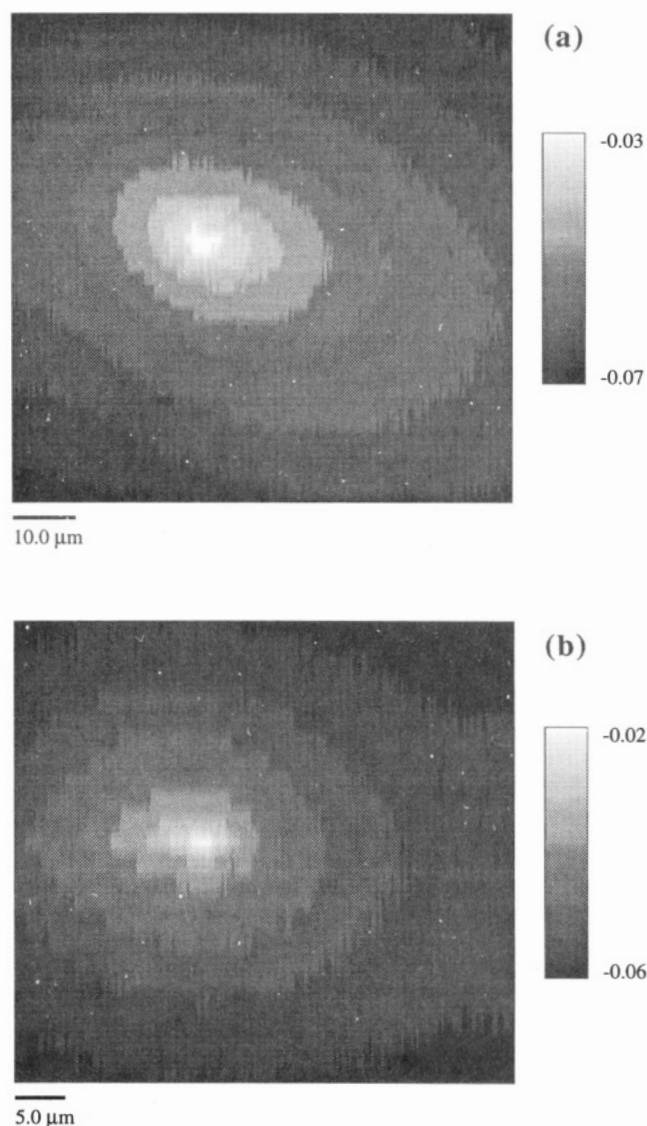


Figure 7. Images of NH_4^+ concentrations around the same target as in Figure 6 at a constant height of (a) 22 and (b) 12 μm from the target surface. Gray scale shows the NH_4^+ ISME potential. White corresponds to a high NH_4^+ concentration. Tip diameter, 1 μm ; scan rate, 1 $\mu\text{m}/\text{s}$; other conditions as in Figure 6.

a 1- μm -diameter tip over the target at a constant height and monitoring the potential. The magnitude of the concentration change was greater when the tip was closer to the target. The concentration contours around the target can also be clearly recognized in these images. In principle, the spatial resolution of an image is governed by the tip radius. However, the resolution can also be affected by voltage resolution in the measuring circuit. For example, if the local concentration change around a target is small, the corresponding potential change may not be resolved. Thus, with smaller tip-to-target separations (i.e., greater concentration changes), a higher resolution image is obtained (compare Figure 7a,b). The apparently discrete concentration contours observed in these images are caused by limitations in the analog-to-digital conversion in the SECM, where small potential changes could not be resolved. As seen in Figure 7b, a resolution of ~ 2 – $3 \mu\text{m}$ was achieved in this case. Similar ion-selective images for concentrations of K^+ and Zn^{2+} around the micropipet targets in 0.1 M NaCl and NH_4Cl solutions, respectively, are shown in Figure 8. Since relatively large tip diameters (20 and 15 μm , respectively)

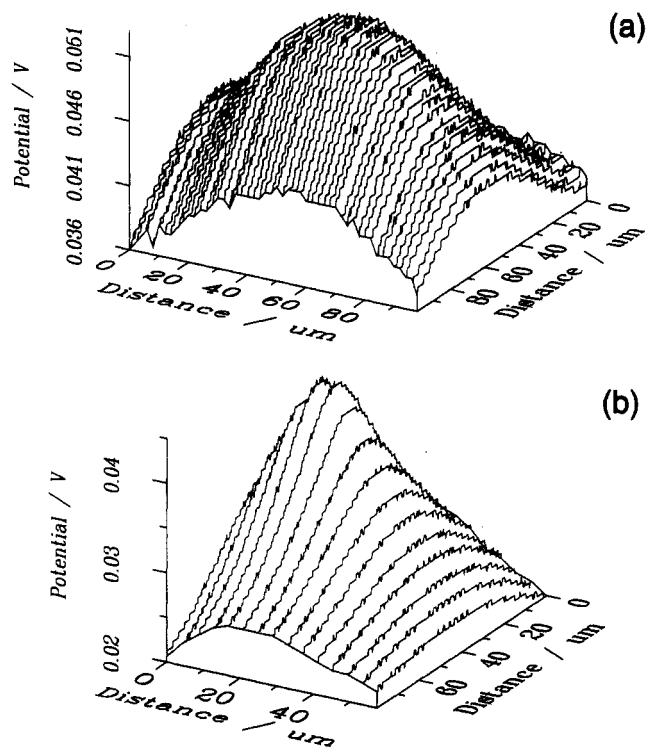
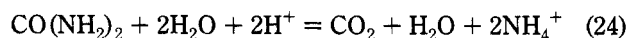


Figure 8. (a) Surface plot of K^+ concentrations around a K^+ source of an 8- μm -diameter micropipet. Tip diameter, 20 μm ; scan rate, 5 $\mu\text{m/s}$; bulk concentration inside the micropipet, 0.1 M KCl; outside, 0.1 M NaCl; applied potential, 0.9 V. (b) Surface plot of Zn^{2+} concentrations around a Zn^{2+} source of a 9- μm -diameter micropipet. Tip diameter, 15 μm ; scan rate, 3 $\mu\text{m/s}$; bulk concentration inside the micropipet, 0.1 M $Zn(NO_3)_2$; outside, 0.1 M NH_4Cl ; applied potential, 0.9 V.

were used here, a lower resolution in the images is observed (compared to that in Figure 7). The overall results demonstrate that the potentiometric SECM can be used for ion-selective imaging with micrometer-level resolution.

Mapping of Local Enzyme Activity. A promising application of potentiometric SECM with ISMEs is the characterization of biologically active sites on a surface, e.g., the mapping of local enzyme activity.^{11,12,16,32} While amperometric SECM can be used with redox enzymes,^{11,12} potentiometric SECM can extend the scope of the application to many other enzymes such as hydrolases.¹⁶ To demonstrate this application, the urease-catalyzed hydrolysis of urea was used as a model system with detection of NH_4^+ . This system was previously employed in a poorly buffered solution with SECM imaging of pH changes with an Sb tip.¹⁶ When a freshly prepared urea solution was introduced into the cell and contacted with the urease target, the hydrolysis of urea occurred,



The NH_4^+ ISME tip was positioned over the urease target at the x - y position of maximum concentration. The z -direction concentration profile of NH_4^+ over the center of a 20- μm -diameter urea target is shown in Figure 9a for a 0.1 M, pH 7, Tris buffer with 0.1 M urea. As expected, a higher concentration of NH_4^+ was found near the urease target. Since urease is reasonably stable and the urea-catalyzed hydrolysis process is not complicated by

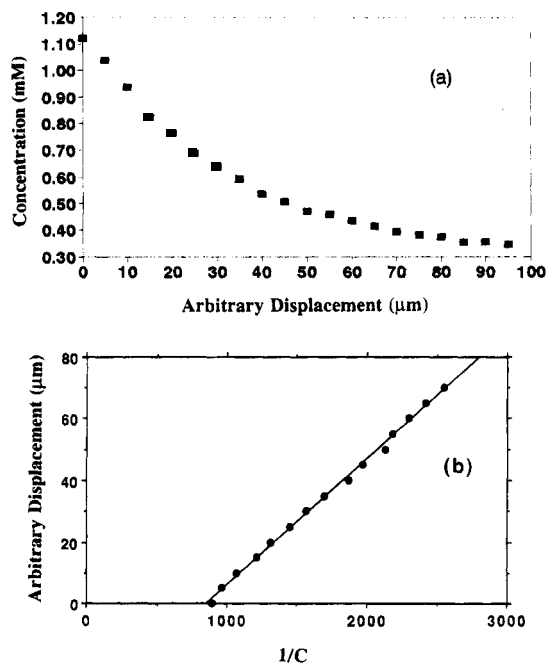


Figure 9. (a) NH_4^+ concentration profile above a 20- μm -diameter urease gel target (in the z -direction) over the center of the target. Tip diameter, 18 μm ; bulk concentration, 0.1 M urea and 0.1 M Tris, pH 7. (b) Plot of arbitrary distance vs $1/c$ using the data in part a.

substrate or product inhibition, with a fixed amount of urease immobilized at the target and excess urea in the solution, the target surface concentration of the generated NH_4^+ should be constant, and the steady-state concentration profile established can be expressed by eq 15. A plot of $1/c$ vs arbitrary displacement using the data in Figure 9a shows the expected linear dependence when the tip electrode is relatively far from the target (i.e., $d > 3r_s$). Thus, eq 18 is valid for a description of the concentration profile in the z -direction over the center of the urease target, and the surface concentration of NH_4^+ can be calculated from the slope in Figure 9b. With $r_s = 10 \mu\text{m}$, the surface concentration of NH_4^+ , C_s , is 6.4 mM, and the flux of NH_4^+ at the surface can be estimated from the following expression:

$$N = 4DC_s r_s \quad (25)$$

Assuming $D = 1.84 \times 10^{-5} \text{ cm}^2/\text{s}$,³³ eq 25 gives $N = 4.7 \times 10^{-13} \text{ mol/s}$. The flux can also be determined without knowing the target radius, since $c_s r_s$ can be directly obtained from Figure 9b (see eq 20).

Surface images for concentrations of NH_4^+ over a 20- μm -diameter urease disk target obtained at a constant height are shown in Figure 10. The concentration of NH_4^+ is also reflected by the circular concentration contours observed. Clearly, the results presented here show that potentiometric SECM with micropipet-based ISMEs can be used to map the distribution of enzyme activity on a surface. In principle, different enzyme sites on a surface could also be mapped, assuming they are sufficiently spaced compared to the tip radius.

Measurements within the Diffusion Layer of a UME.

When a soluble electroactive species is electrochemically reduced or oxidized, a concentration profile of the reactant is built up near

(32) Wang, J.; Wu, L.; Li, R. J. *Electroanal. Chem.* 1989, 272, 285.

(33) Lobo, V. M. M. *Handbook of Electrolyte Solutions*; Elsevier: New York, 1989; Part B.

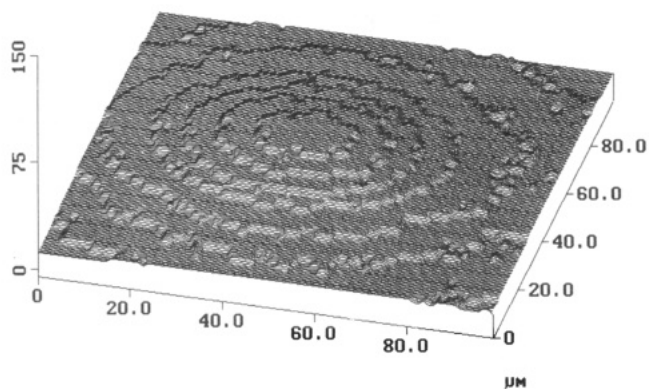


Figure 10. Surface plot of NH_4^+ concentrations around the same target as in Figure 9a at a constant height of $\sim 35 \mu\text{m}$ from the target surface. Tip diameter, $18 \mu\text{m}$; scan rate, $5 \mu\text{m/s}$; solution, as in Figure 9. Units in the z -direction are arbitrary.

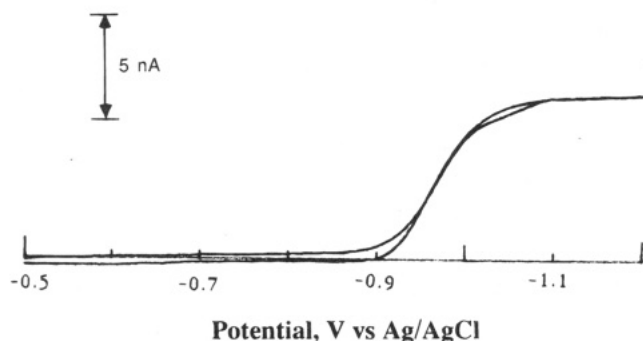
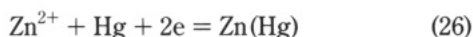


Figure 11. Cyclic voltammogram of a $25\text{-}\mu\text{m}$ -diameter Hg-coated Au electrode in $0.84 \text{ mM Zn}(\text{NO}_3)_2$, $0.1 \text{ M NH}_4\text{Cl}$, and $50 \text{ mM pH } 7$ Tris buffer. Scan rate, 10 mV/s .

the electrode surface. If a microdisk target electrode with a radius below $10\text{--}20 \mu\text{m}$ is used, the concentration profile reaches a steady state in a time of the order of tens of r_s^2/D , and the established diffusion layer is rather thin, usually with a thickness of a few electrode diameters. Experimental measurement of the steady-state concentration profile (given by eq 21) near an electrode is difficult because of the small thickness of the diffusion layer. Although the SECM with amperometric tips has been used to probe the diffusion layer,³⁴ these tips can perturb the concentration profile being examined because of the electrochemical reaction occurring at the tip which consumes the species being determined. An inert potentiometric probe is better, although blocking by the tip still causes some perturbation of the profile. As a model system, we chose the electrochemical reduction of Zn^{2+} at a Hg-coated Au microdisk electrode ($25\text{-}\mu\text{m}$ diameter), probing the Zn^{2+} concentration profile with a Zn^{2+} -selective microelectrode. A cyclic voltammogram of the Hg-coated Au electrode in 50 mM Tris buffer, $\text{pH } 7$, containing $0.84 \text{ mM Zn}(\text{NO}_3)_2$ and $0.1 \text{ M NH}_4\text{Cl}$ (Figure 11) shows a current plateau at $-1.0 \text{ V vs Ag/AgCl}$ associated with the reduction of Zn^{2+} ,



This reaction occurred well before the background hydrogen evolution reaction. To generate a Zn^{2+} concentration profile, the

(34) Engstrom, R. C.; Weber, M.; Wunder, D. J.; Burgess, R.; Winquist, S. *Anal. Chem.* **1986**, *58*, 844.

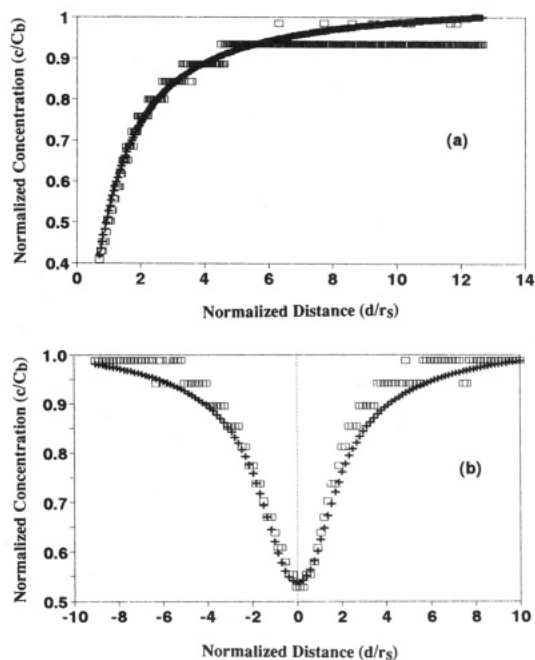


Figure 12. Zn^{2+} concentration profile above a $25\text{-}\mu\text{m}$ -diameter Hg-coated Au electrode (a) in the z -direction over the center of the electrode and (b) in the radial direction across the center of the electrode at a constant height of $11 \mu\text{m}$ from the surface. Electrode potential was held at -1.15 V . Tip diameter, $10 \mu\text{m}$; scan rate, $2 \mu\text{m/s}$; solution, same as in Figure 11. \square , Experimental data; $+$ $+$ $+$, theoretical curves.

target was held at $-1.15 \text{ V vs Ag/AgCl}$, where the electroreduction of Zn^{2+} was diffusion-controlled. A Zn^{2+} ISME was then placed within the diffusion layer and scanned over the target for the concentration measurement. The Zn^{2+} ISME was positioned in the $x\text{-}y$ plane at the point of lowest concentration of Zn^{2+} , corresponding to the center of the target. The normalized concentration profile of Zn^{2+} as a function of the normalized distance in the z -direction over the center of the target is shown in Figure 12a. Figure 12b gives the dependence of the concentration on the radial position while the tip was scanned across the center of the target along the x -dimension at a constant height of $11 \mu\text{m}$ from the target surface. The squares show the experimental data, and the pluses are the theoretical points calculated from eqs 22 (Figure 12a) and 23 (Figure 12b). The experimentally determined concentration profiles were in good agreement with the theory in both cases. No significant perturbation of the concentration profile by the tip presence or movement was observed, probably because the steady state at the UME was established rapidly and the tip dimension was relatively small. Note, however, that sensitivity limitations of the measuring A/D converter of the SECM system led to an inability to resolve the differences in concentration in the higher concentration region. This problem was more severe with divalent ions, since $\Delta E/\Delta \log c$ is smaller compared to that for monovalent ions.

Figure 13 shows a gray scale image of the Zn^{2+} concentration above the target; a lower concentration (dark area) is observed over the center of the target where Zn^{2+} was consumed. The observed target current increased slowly as the reaction in eq 26 proceeded. This was probably due to a continuous increase of the electrode surface area by the electrodeposition of zinc at the target. This accumulation of zinc at the target could also cause a decrease in the distance between the tip and target. However,

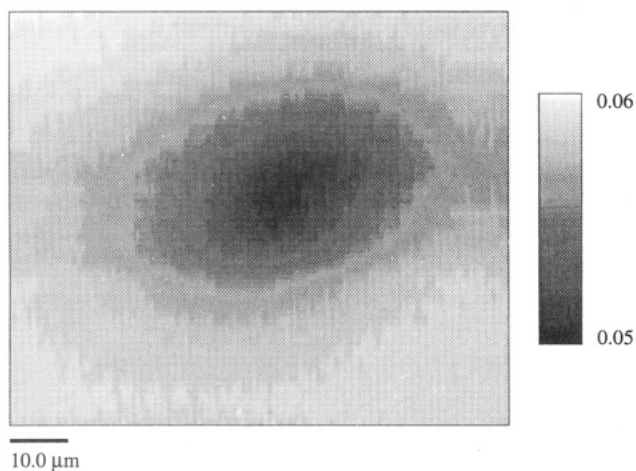


Figure 13. Image of Zn^{2+} concentrations around the same target as in Figure 12 at a constant height of $\sim 11 \mu\text{m}$ from the surface. Gray scale shows the Zn^{2+} ISME potential; black corresponds to a low Zn^{2+} concentration. Other conditions as in Figure 12.

this effect was negligible within the time frame for potentiometric imaging.

CONCLUSIONS

In this study, the general methodology for potentiometric SECM based on the use of micropipet ISMEs was established. The results demonstrated the ability of these to image local concentrations of ions with micrometer resolution. Potentiometric SECM was also used to map local enzyme activity and to perform measurements within the diffusion layer of a UME. A particular advantage for potentiometric SECM with ISME tips is its applicability in determining the local concentrations of electroinactive species, which can lead to application in biological systems. Other advantages for ISME tips are their good selectivity and their nature as passive sensors. The difficulty in the determination of the absolute tip position in potentiometric SECM was overcome by using dual-channel tips in which one channel worked as an ISME and the other as a distance sensor. In these, the distance sensor was a Ag/AgCl micropipet electrode, and the experimental data were found to be in good agreement with theory. For a system at steady state, the measured concentration profile could also be employed to estimate the absolute tip-to-target distance using the corresponding diffusion model. The quantitative analysis of the concentration profile around different targets was in reasonable agreement with theoretical predictions.

ACKNOWLEDGMENT

Financial support of this work by the National Science Foundation (CHE9214480) and the Robert A. Welch Foundation is gratefully acknowledged. We also appreciate helpful discussions with F.-R. F. Fan, B. R. Horrocks, and H. S. White.

LIST OF SYMBOLS

a	tip radius (μm)
C	dimensionless concentration
c	concentration (mol cm^{-3})
C_b	bulk concentration (mol cm^{-3})
C_{dl}, C_{dl}'	double-layer capacitance of electrode (F)
C_s	surface concentration (mol cm^{-3})
D	diffusion coefficient ($\text{cm}^2 \text{s}^{-1}$)
d	absolute tip-to-substrate distance (μm)
d'	arbitrary displacement distance (μm)
E	electrode potential (V)
F	Faraday constant
h	tip length of micropipet (mm)
i_T	tip current (A)
$i_T(L)$	feedback current of a microdisk at the normalized tip-to-substrate distance L
$i_{T,\infty}$	tip current when tip is far from the substrate (A)
j	current density (A cm^{-2})
L	normalized tip-to-substrate distance equal to d/a
L'	dimensionless tip-to-substrate distance equal to d/r_s
N	flux of species at a surface, equal to $4DC_s a$
n	number of electrons transferred per redox event
R	dimensionless radial distance, r/r_s
r	radial variable
r_0	radius of tip capillary tube (mm)
R_{ct}, R_{ct}'	charge-transfer resistance of electrode (Ω)
RG	ratio of glass sheath diameter to electrode diameter
r_s	target radius (μm)
R_{sol}	external solution resistance between micropipet and reference electrodes (Ω)
$R_{sol}(L)$	external solution resistance as a function of L
$R_{sol,\infty}$	$R_{sol}(L)$ with the tip far from the substrate
R_t	total solution resistance (Ω)
$R_t(L)$	total solution resistance as a function of L
$R_{t,\infty}$	total solution resistance with tip far from substrate
R_{tip}	solution resistance inside micropipet electrode (Ω)
z	axial variable
$\Delta R(L)$	difference between $R_t(L)$ and $R_{t,\infty}$
κ	solution conductivity (S cm^{-1})
ρ	solution resistivity (Ωcm)
ϕ	electrostatic potential (V)

Received for review August 22, 1994. Accepted February 5, 1995.[®]

AC940829U

[®] Abstract published in *Advance ACS Abstracts*, March 15, 1995.